RSC Advances

PAPER

View Article Online
View Journal | View Issue

Cite this: *RSC Adv.*, 2014, **4**, 30392

Waveguide based energy transfer with gold nanoclusters for detection of hydrogen peroxide

T. N. Lin,[a] Y. L. Chang,[a] G. W. Shu,[a] C. T. Yuan,[a] J. L. Shen,*[a] C. H. Chiu,[b] H. C. Kuo,[c] C. A. J. Lin,[d] W. H. Chang,[d] H. H. Wang,[e] C. H. Su[e] and H. I. Yeh[e]

Received 8th April 2014
Accepted 27th June 2014

DOI: 10.1039/c4ra03153a

www.rsc.org/advances

H_2O_2 detection that uses fluorescence resonance energy transfer from InGaN quantum wells to Au nanoclusters *via* optical waveguiding has been developed. Steady and time-resolved photoluminescence studies have been used to demonstrate the waveguide-based energy transfer. H_2O_2 detection is achieved by the quenching of the red emission from Au nanoclusters. Advantages of the sensing technique include the capability of visual detection and large area analysis.

1. Introduction

Gold nanoclusters (NCs) with a typical size of less than ~2 nm are highly attractive due to their particular dimension between metal atoms and nanoparticles. The quantized confinement effects of the Au NCs result in discrete and size-tunable electronic transitions, leading to molecular-like luminescence and unique charge properties. These novel properties have been utilized in the field of colloidal chemistry, cluster science, biomedicine, and optoelectronics.[1–5] The surfaces of Au NCs can be easily functionalized with various organic and biomolecular ligands, among which the protein molecules have attained much attention for their facile synthesis, low toxicity, high quantum yield, and good photostability.[6–9] In addition, the protein-stabilized Au NCs generally has low tissue absorption and scattering effects in the near-infrared region. All of these properties in the protein-stabilized Au NCs show that they can be used as promising fluorescent probes and utilized in the biomedical applications for sensing, catalysis, imaging, and labeling.[6,9] Förster or fluorescence resonance energy transfer (FRET), a process involving the nonradiative energy transfer between two nearby fluorophores, is a promising technique to optically detect molecular binding events.[10,11] FRET occurs when there is appreciable overlap between the emission spectrum of donors and the absorption spectrum of acceptors, and its efficiency strongly depends on the distance of separation between donors and acceptors. FRET combines the sensitivity of fluorescence measurement with a strong distance dependence that is an ideal tool for chemical or biological sensing.[11] The donor and the acceptor can be brought together to produce FRET in several ways. For example, the donors and the acceptors are simultaneously attached to a molecule at close positions to interact. An alternative type of FRET is the energy transfer between a semiconductor quantum well (QW) and an overlay of acceptors, which has been theoretically predicted at the late 1990s.[12] This type of FRET provides a nonradiative pumping route to electrical carrier injection that overcomes the losses imposed by the associated low carrier mobility of acceptor materials.[13,14] The experimental evidences of resonance energy transfer according to the above mechanism have been experimentally demonstrated between the III-nitride quantum-well donor and the nanomaterial acceptor.[13–16]

Recently, we have designed and built a new type of energy transfer to combine FRET with optical waveguides.[17] The configuration is based on multiple total internal reflection of an incident laser within the semiconductor material, such that the quantum-well donor can interact with the acceptor on top of the semiconductor surface. An important benefit of this configuration is that the acceptor is excited solely by energy transfer from the donor, avoiding unwanted excitation from the incident light and leading to an accurate energy transfer efficiency. In addition, by the principle of the total internal reflection, the resonant light can travel along in a waveguide and hence produce a large interaction area between the donor and the acceptor. The waveguide-based FRET has been demonstrated at low temperatures by the photoluminescence (PL) using an InGaN quantum-well (QW) donor paired with an Au NC acceptor.[17] With the advantages of rapid direct response and large area detection, the energy transfer *via* optical waveguides could be introduced as transducers for FRET-base (bio)sensors. In this work, we perform PL measurements to study the FRET from InGaN QWs to Au NCs *via* optical waveguides for sensing hydrogen peroxide (H_2O_2). A conceptual design of such an

[a]*Physics Department, Chung Yuan Christian University, Chung-Li, Taiwan. E-mail: jlshen@cycu.edu.tw*

[b]*Advanced Optoelectronic Technology Inc., Hsinchu, Taiwan*

[c]*Department of Photonic and Institute of Electro-Optical Engineering, National Chiao Tung University, Hsinchu, Taiwan*

[d]*Department of Biomedical Engineering, Chung Yuan Christian University, Chung-Li, Taiwan*

[e]*Department of Medical Research, Mackay Memorial Hospital, Mackay Medical College, New Taipei City, Taiwan*

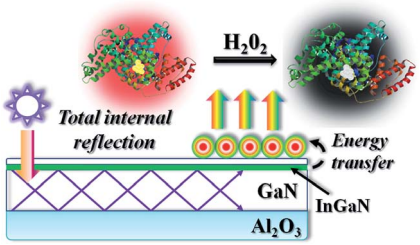

Fig. 1 Schematic illustration of the detection of H_2O_2 using the waveguide-based energy transfer from InGaN quantum wells (QWs) to Au nanoclusters (NCs).

waveguide-based FRET is schematically shown in Fig. 1. The detection of H_2O_2 is very important since H_2O_2 plays an essential role in some enzymatic reactions, as well as being a significant intermediate in biological and environmental monitoring. The PL of the Au NC acceptors was found to decrease rapidly after introducing H_2O_2. The quenching of luminescence intensity was related to the concentration of H_2O_2. On the basis of the time-resolved PL studies, we suggest that the incorporation of H_2O_2 triggers an oxidation of Au–S bonding in Au NCs, leading to a luminescence quenching of acceptors in FRET. The waveguide-based FRET could provide a single surface for the patterning of large-area multiple molecules, allowing for further development of multiplexed biosensors that facilitates visual detection.

2. Experimental section

The donor used for the present study is a single InGaN/GaN QW structure grown by metal–organic chemical vapor deposition on a double-side polished (0001)-oriented sapphire substrate. After a 2 μm thick GaN buffer layer on the substrate, a single InGaN QW layer with thickness of 2 nm was grown. The growth is terminated by a 2 nm thick GaN cap layer. The acceptor in this study is the bovine serum albumin (BSA) template Au NCs developed by Ying *et al.*[18] The BSA-stabilized Au NCs were synthesized by chemical reduction of $HAuCl_4$ with BSA according to ref. 18. Briefly, $HAuCl_4$ solution (20 mL, 10 mM) was added into BSA solution (20 mL, 50 mg mL^{-1}) under vigorous stirring. After 2 minutes, NaOH solution (2 mL, 1 M) was introduced, and the mixture was incubated at 37 °C for 12 h and the color of the solution changed from light yellow to deep brown. To perform the FRET experiment, an Au NC (acceptor) was incorporated on the top of an InGaN QW (donor) by the drop-casting method. A pulsed laser with a wavelength of 260 nm, a repetition frequency of 20 MHz, and a duration of 250 fs was used as the excitation source. The collected luminescence was projected into a spectrometer and detected with a high-speed photomultiplier tube (PMT). Time-resolved PL were performed using the technique of time-correlated single-photon counting (TCSPC). The instrument response of the time-correlated single photon counting system is about 250 ps. All the measurements were carried out at room temperature.

3. Results and discussion

The optical properties of the energy donor and acceptor were characterized using PL and photoluminescence excitation (PLE) spectroscopy. The solid line in Fig. 2(a) shows the PL spectrum of the InGaN QW (donor), revealing a narrow PL band that peaks at around 450 nm. On the other hand, the squares and circles in Fig. 2(a) show the PL and PLE spectrum of the Au NC (acceptor), respectively. The BSA-stabilized Au NCs show a PL band at 670 nm. Referred to previous studies, the PL band originates from molecular-like transitions between the highest occupied molecular orbital (HOMO) to lowest unoccupied molecular orbital (LUMO) in Au NCs.[9] The PLE spectrum of Au NCs exhibits a strong absorption band at ~330 nm and a weak absorption band at ~500 nm. The good spectral overlap between the donor InGaN QWs and the acceptor Au NCs indicates the feasibility of FRET between them. The solid and dashed line in Fig. 2(b) shows the PL spectrum of the donor InGaN QW in the presence and absence of the acceptor Au NCs, respectively. A decrease of the relative donor PL intensity and a simultaneous increase in the acceptor PL emission was observed in the presence of acceptors. This observation demonstrates the energy transfer from InGaN quantum wells to Au NCs. The existence of FRET can be further identified by measuring the time-resolved PL. If the energy transfer is mediated through a nonradiative process, a decrease of the donor lifetime should be observed. On the other hand, if the acceptor is pumped radiatively by the emission of donors, its lifetime should remain unchanged. The triangles and circles in the inset of Fig. 2(b) show the PL decay profiles of the InGaN QW structure in the presence and absence of Au NCs, respectively. Evidently, the decay time from InGaN QWs in the presence of the Au NCs decreases considerably, in agreement with the behavior of FRET.

The PL decays of InGaN QW obtained above can be used to estimate the energy transfer efficiency. The PL decay of the InGaN QW is expected to be characterized by a distribution of lifetimes owing to the indium phase segregation and the indium fluctuation.[19] Thus, the PL decay curves in the inset of Fig. 2(b) were fitted by the stretched exponential function:

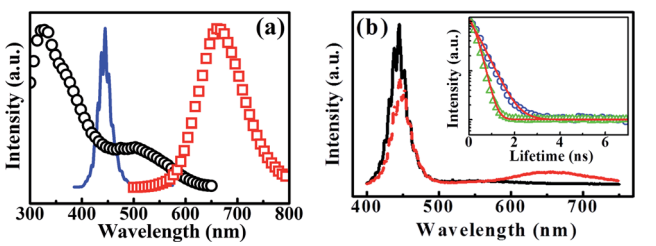

Fig. 2 (a) Photoluminescence (PL) spectra of the InGaN QW (solid line) and the Au NCs (squares) and PL excitation spectrum of the Au NCs (circles). (b) The PL spectra of the InGaN QW in the presence (the dashed line) and absence (the solid line) of Au NCs. The inset shows PL decay profiles of the InGaN QW in the presence (triangles) and absence (circles) of Au NCs. The solid lines in the inset are the fitted curves using eqn (1).

$$I(t) = Ae^{-(t/\tau)^{\beta}}, \quad (1)$$

where τ represents the decay time of decay, A represents the amplitude of the decay component at $t = 0$. The solid lines in the inset of Fig. 2(b) show the fitted curves using eqn (1), replicating well with the experimental results. In the stretched exponential function the average decay time is calculated as follows:[20]

$$\langle\tau\rangle = \frac{1}{k\beta}\Gamma\left(\frac{1}{\beta}\right), \quad (2)$$

where Γ is the mathematical Gamma function. It is expected that the nonradiative energy transfer leads to a change in the decay dynamics of the InGaN QW. In the absence of Au NCs, the PL decay rate of the bare QW is represented by $\langle\tau_{QW}\rangle^{-1}$. After introducing with Au NCs, the PL decay rate of the QW in the hybrid sample can be described by the following equation:

$$\langle\tau_{hybrid}\rangle^{-1} = \langle\tau_{QW}\rangle^{-1} + \langle\tau_{ET}\rangle^{-1}, \quad (3)$$

where $\langle\tau_{ET}\rangle$ represents the characteristic time of the energy transfer process. The energy-transfer efficiency Φ_{ET} is the fraction of the photons absorbed by the donor that are transferred to the acceptor and can be expressed by:

$$\Phi_{ET} = \frac{\langle\tau_{ET}\rangle^{-1}}{\langle\tau_{QW}\rangle^{-1} + \langle\tau_{ET}\rangle^{-1}}, \quad (4)$$

From eqn (1)–(3), the calculated $\langle\tau_{QW}\rangle$, $\langle\tau_{hybrid}\rangle$, and $\langle\tau_{ET}\rangle$ were determined to be 0.53, 0.36, and 1.1 ns, respectively. The above values allow us to estimate Φ_{ET} and a value of ~37% was obtained.

The top-view photograph of the investigated sample is depicted in the Fig. 3(a) upon optical excitation according to the configuration in Fig. 1. A red-light image with an area of ~6.3 cm^2 was clearly seen in the region where Au NCs were drop-casted, about 1 cm away from the laser excitation spot. The image in Fig. 3(a) was obtained without the use of an emission filter (normally used to filter out the light from the excitation source in the conventional FRET). Thus, the emitted red light can be directly seen by a naked eye. This result indicates that our waveguide-based platform can be a transducer for the fluorescence-based sensor. The effect of H_2O_2 on the FRET of the hybrid InGaN QW/Au NC sample was investigated. Fig. 3(b) and (c) show the images of the hybrid sample by introduction of H_2O_2 with the concentrations of 100 mM and 1 M, respectively. The red emission of Au NCs in the hybrid sample quenches gradually with increasing the concentration of H_2O_2. Over 90% fluorescence was quenched by the addition of H_2O_2 with the concentration of 1 M and the quenching effect had good reproducibility. From the above results, the quenching response of fluorescence in Au NCs is sensitive after introduction of H_2O_2. Thus, it can provide a new strategy for the visual detection of H_2O_2 by using the wave-guided platform designed in Fig. 1.

To understand the reaction time of the above quenching effect, time-dependent PL experiments for Au NCs in the presence of H_2O_2 were performed. As shown in Fig. 4, the PL intensity of the Au NCs was constant in time in the absence of H_2O_2. After introducing H_2O_2, the PL is quenched over 85% in less than 150 s and thus indicates a quick process. The quick quenching response is beneficial for monitoring H_2O_2 in sample. One geometric factor which influences the sensitivity of

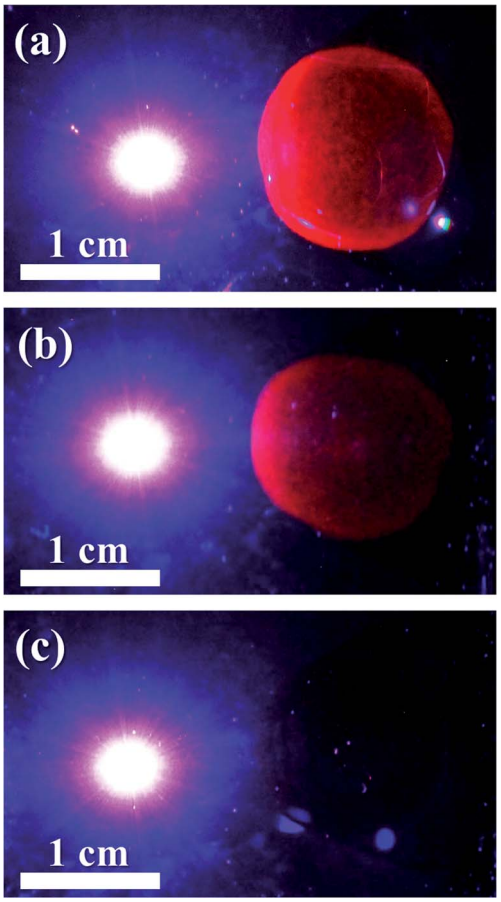

Fig. 3 The images of the hybrid InGaN QW/Au-NC sample upon excitation of an UV laser with the concentration of H_2O_2: (a) 0; (b) 100 mM; (c) 1 M. The left bright spot in each image is caused by the excitation laser.

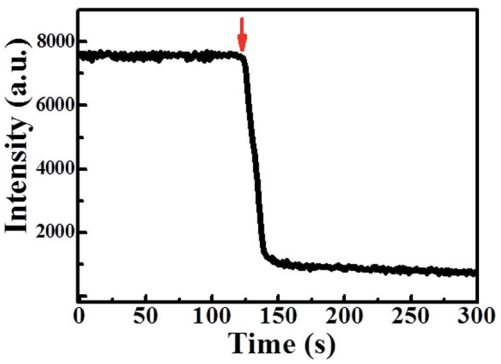

Fig. 4 The PL intensity of Au NCs *versus* time with addition of H_2O_2. The arrow indicates the time when H_2O_2 was introduced.

PL in our system is the separate distance between the laser excitation spot and Au NCs. The effect of separate distance on the PL in Au NCs was characterized by fixing the detection position and moving the excitation spot. Fig. 5 shows the PL spectra of Au NCs as a function of the separation distance between the laser excitation spot and Au NCs. As the separation distance increases, the PL intensity decreases pronouncedly. The separation distance *versus* the PL intensity in Au NCs is shown in the inset of Fig. 5, indicating a linear relationship. The information of the distance dependence between the laser spot and Au NCs is useful for simultaneous measurements of multiple samples on a single chip. Thus, the waveguide-based method in our design can provide benefits include large area analysis as well as multicolor sensing.

To find out mechanism of the luminescence quenching by H_2O_2, time-resolved PL investigations with different concentrations of H_2O_2 were carried out. Fig. 6 shows the PL decay profiles of the 670 nm peak from the hybrid sample with different concentrations of H_2O_2. These PL decays were well described by a double-exponential function:

$$I(t) = A_f e^{-\frac{t}{\tau_f}} + A_s e^{-\frac{t}{\tau_s}}, \quad (5)$$

where $\tau_f(\tau_s)$ represents the decay time of fast (slow) decay, $A_f(A_s)$ represents the amplitude of the fast-decay (slow-decay) component at $t = 0$. The solid lines of Fig. 6 show the fitted curves using eqn (5). With increasing the concentration of H_2O_2, the decay time (~3.2 ns) and amplitude (~0.85) of the fast component in PL decays remain basically unchanged. (Table 1) On the other hand, the amplitude of the slow component decreases pronouncedly (from 0.2 to 0.08) with increasing concentration of H_2O_2 while the decay time of the slow component keeps constant (~120 ns) (Table 1). This result indicates that introduction of H_2O_2 only affect the slow-decay component of the PL decays in Au NCs. According to previous studies, the BSA-stabilized Au NCs have a core-shell structure where 13 Au atoms form an icosahedral core surrounded by six semiring S–Au–S–Au–S bonding (staple motifs).[9,21] The staple motifs have been found to be responsible for the slow-decay process of luminescence in the BSA-stabilized Au NCs.[21] Thus,

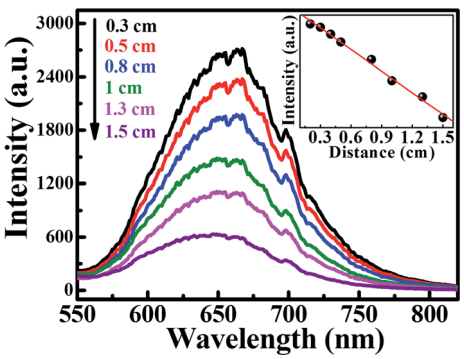

Fig. 5 The luminescence spectra of the hybrid InGaN QW/Au NC sample by changing the separation distance between the laser excitation spot and Au NCs. The inset shows the luminescence intensity as a function of separation distance.

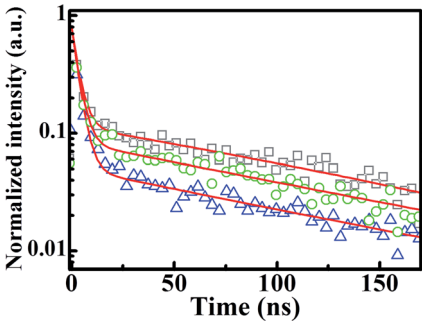

Fig. 6 The PL decay profiles of the 670 nm peak in Au NCs with the concentrations of H_2O_2: 0 (squares); 1 mM (circles); 100 mM (triangles). The solid lines are the fitted curves using eqn (5).

Table 1 The decay time of fast (slow) decay $\tau_f(\tau_s)$ and the amplitude of the fast-decay (slow-decay) component $A_f(A_s)$ used in the fits according to eqn (5)

	A_f (%)	τ_f (ns)	A_s (%)	τ_s (ns)
Au@BSA	80	3.22	20	124.4
H_2O_2 (1 mM)	84	3.19	16	120.9
H_2O_2 (100 mM)	92	3.16	8	116.0

the major effect of H_2O_2 is to interact with the staple motifs in the BSA-stabilized Au NCs, associated with the slow component in PL decays. Based on the finding, we suggest that the Au–S bonds within the staple motifs could be oxidized by the strong oxidant H_2O_2 and forms an organic disulfide product (RS-SR).[22,23] Owing to the H_2O_2-mediated oxidation and a decrease of the density of the Au–S bonds, the ability to donate electron density to the Au NC surface reduces, leading to a disappearance of the red emission from the hybrid sample.

To confirm the quenching of luminescence in Au NCs is caused by oxidation of Au NCs, the effect of other oxidizing agents on the PL of Au NC sample was investigated. Fig. 7 shows the PL spectra of Au NCs by introducing Ammonium persulfate (APS) and Potassium dichromate (K_2CrO_7). The PL spectra display a clear quenching in PL intensity after adding APS (10 mM) and K_2CrO_7 (10 mM). This indicates the oxidation of Au–S

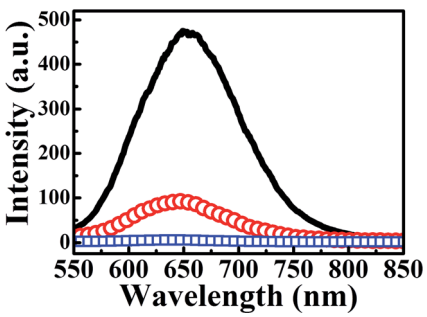

Fig. 7 The PL spectra of Au NCs in the absence (solid line) and presence of ammonium persulfate (APS) (circles) and potassium dichromate (K_2CrO_7) (squares).

is not specific to H_2O_2, many oxidizing agents can be quenchers. It is interesting to understand whether PL quenching in Au NCs is reversible. The reducing agent sodium borohydride ($NaBH_4$) were used to test the reversibility of the PL quenching in Au NC sample. Fig. 8 shows the PL spectra of Au NCs by introducing $NaBH_4$ (10 mM) to the Au NCs, which has been oxidized by H_2O_2 (10 mM). After Adding the $NaBH_4$ to the H_2O_2-oxidized Au NC sample, the PL recovered pronouncedly and rapidly. From the results of Fig. 7 and 8, we confirm that the quenching mechanism of PL in Au NCs in the presence of H_2O_2 is due to the oxidation effect, as suggested previously.

Considering the significant quenching in the luminescence intensity, the possibility of developing a sensitive method for detecting H_2O_2 has been evaluated. Changes of the luminescence intensity of Au NCs *versus* the concentration of H_2O_2 are shown in Fig. 9. With the increase of H_2O_2 concentration the PL spectra displayed a gradual decrease in luminescence intensity without any change in the wavelength of emission. The relative luminescence intensity (I_0/I, where I and I_0 were the luminescence intensity in the presence and absence of H_2O_2, respectively) as a function of H_2O_2 concentration is displayed in Fig. 10. It is obvious that the dependence of H_2O_2 concentration on the PL quenching results in two distinct regimes. For high concentration of H_2O_2 (C > 10 mM), there is a linear relationship between the magnitude of luminescence quenching and the H_2O_2 concentration. The magnitude of luminescence

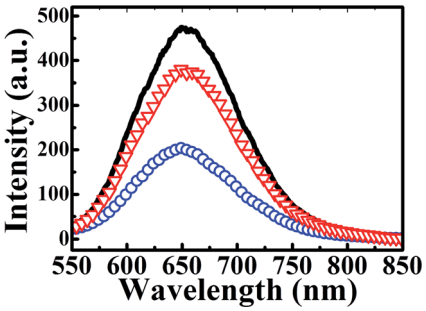

Fig. 8 The PL spectra of the H_2O_2-oxidized Au NCs in the absence (circles) and presence of $NaBH_4$ (triangles). The solid line shows the PL spectra of Au NCs before H_2O_2-oxidization.

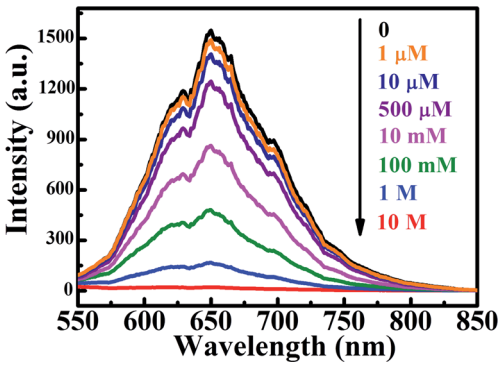

Fig. 9 The luminescence spectra of the hybrid InGaN QW/Au NC sample by adding H_2O_2 with different.

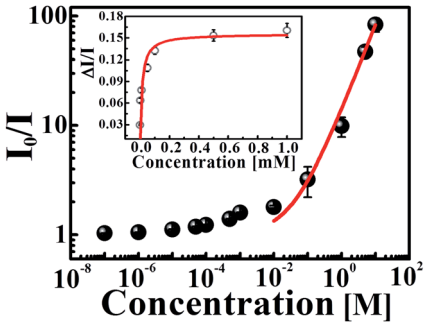

Fig. 10 The dependence of luminescence quenching in the hybrid InGaN QW/Au NC sample on the concentration of H_2O_2. The solid line is the fits according to eqn (6). The inset shows the dependence of luminescence quenching for H_2O_2 concentrations ≦1 mM. The solid line in the inset is the fits according to eqn (7).

quenching as a function of the concentration can be described using a modified Stern-Volmer equation:[24]

$$\frac{I_0}{I} = 1 + K_{SV}[C]^a, \quad (6)$$

where K_{SV} is the Stern-Volmer coefficient which reflects the quenching efficiency and a is a constant. The solid line in Fig. 10 shows the fits according to eqn (6) with $K_{SV} = 13.2\ M^{-1}$ and $a = 0.79$. The good overlap between the experimental data and the fit indicates the luminescence quenching and the H_2O_2 concentration is linear for high concentrations (C > 10 mM). On the other hand, the luminescence intensity decreases a little from 10 mM to 0.1 μM for the low concentrations (C < 10 mM). The inset of Fig. 10 shows the relative luminescence intensity in Au NCs after the addition of H_2O_2 with different concentrations. It was found that the effect of H_2O_2 on the change of fluorescence intensity can be correlated with Langmuir isotherm:[25]

$$\frac{I_0 - I}{I} = A\frac{K \times C}{1 + K \times C}, \quad (7)$$

where A and K are Langmuir constants. Using eqn (7). The solid line in the inset of Fig. 10 displays the calculated result with $A = 0.15$ and $K = 8.07 \times 10^4$. A good fit to experiment is found, indicating the PL quenching in the low concentration range is related to surface association phenomena.[25]

4. Conclusions

In summary, we have investigated the detection of H_2O_2 using the waveguide-based FRET from InGaN QWs to the BSA-stabilized Au NCs. There is a decrease of the PL intensity and a shortening of PL decay time for the InGaN QW in the presence of Au NCs, demonstrating a resonance energy from InGaN QWs to Au NCs *via* optical waveguiding. The PL intensity from Au NCs was obviously quenched by the addition of H_2O_2, which may be explained by the H_2O_2-mediated oxidation of the Au–S bonds in the staple motifs in the BSA-stabilized Au NCs. With the advantages of large-area detection and capability of visual detection, the proposed waveguide-based FRET from InGaN QWs to Au NCs could be potentially used as a convenient probe to detect H_2O_2.

Acknowledgements

This project was supported in part by the National Science Council under the grant numbers NSC 102-2627-M-033-002 and NSC 102-2627-M-033-001, and Center for Biomedical Technology in CYCU.

References

1 H. G. Boyen, G. Kästle, F. Weigl, P. Ziemann, G. Schmid, M. G. Garnier and P. Oelhafen, *Phys. Rev. Lett.*, 2004, **87**, 276401.
2 G. Hodes, *Adv. Mater.*, 2007, **19**, 639–655.
3 J. F. Parker, C. A. Fields-zinna and R. W. Murray, *Acc. Chem. Res.*, 2010, **43**, 1289–1296.
4 Z. Wu and R. Jin, *Nano Lett.*, 2010, **10**, 2568–2573.
5 R. Jin, Y. Zhu and H. Qian, *Chem.–Eur. J.*, 2011, **17**, 6584–6593.
6 P. L. Xavier, K. Chaudhari, A. Baksi and T. Pradeep, *Nano Rev.*, 2012, **3**, 14767.
7 F. Samari, B. Hemmateenejad, Z. Rezaei and M. Shamsipur, *Anal. Methods*, 2012, **4**, 4155–4160.
8 K. S. Park, M. I. Kim, M. A. Woo and H. G. Park, *Biosens. Bioelectron.*, 2013, **45**, 65–69.
9 D. M. Chevrier, A. Chatt and P. Zhang, *J. Nanophotonics*, 2012, **6**, 064504.
10 T. Förster, *Ann. Phys.*, 1948, **2**, 55–75.
11 J. R. Lakowicz, *Principle of Fluorescence Spectroscopy*, Kluwer Academic Plenum, New York, 2nd edn, 1999.
12 D. Basko, G. C. La Rocca, F. Bassani and V. M. Agranovich, *Eur. Phys. J. B*, 1999, **8**, 353–362.
13 G. Itskos, C. R. Belton, G. Heliotis, I. M. Watson, M. D. Dawson, R. Murray and D. D. C. Bradley, *Nanotechnology*, 2009, **20**, 275207.
14 S. Chanyawadee, P. G. Lagoudakis, R. T. Harley, D. G. Lidzey and M. Henini, *Phys. Rev. B: Condens. Matter Mater. Phys.*, 2008, **77**, 193402.
15 C. R. Belton, G. Itskos, G. Heliotis, P. N. Stavrinou, P. G. Lagoudakis, J. Lupton, S. Pereira, E. Gu, C. Griffin, B. Guilhabert, I. M. Watson, A. R. Mackintosh, R. A. Pethrick, J. Fedmann, R. Murray, M. D. Dawson and D. D. C. Bradley, *J. Phys. D: Appl. Phys.*, 2008, **41**, 094006.
16 G. Heliotis, G. Itskos, R. Murray, M. D.Dawson, I. M. Watson and D. D. C. Bradley, *Adv. Mater.*, 2006, **18**, 334–338.
17 G. W. Shu, C. C. Lin, H. T. Lin, T. N. Lin, J. L. Shen, C. H. Chiu, Z. Y. Li, H. C. Kuo, C. C. Lin, S. C. Wang, C. A. J. Lin and W. H. Chang, *Opt. Express*, 2011, **19**, A194–A200.
18 J. Xie, Y. Zheng and J. Y. Ying, *J. Am. Chem. Soc.*, 2009, **131**, 888–889.
19 M. Pophristic, F. H. Long, C. Tran, I. T. Ferguson and R. F. Karlicek Jr, *J. Appl. Phys.*, 1999, **86**, 1114–1118.
20 A. F. van Driel, I. S. Nikolaev, P. Vergeer, D. Vanmaekelbergh and W. L. Vos, *Phys. Rev. B: Condens. Matter Mater. Phys.*, 2007, **75**, 035329.
21 X. Wen, P. Yu, Y. R. Toh, A. C. Hsu, Y. C. Lee and J. Tang, *J. Phys. Chem. C*, 2012, **116**, 19032–19038.
22 D. O. de O. Lucana, I. Wedderhoff and M. R. Groves, *J. Signal Transduction*, 2012, **2012**, 605905.
23 X. Xia, Y. Long and J. Wang, *Anal. Chim. Acta*, 2013, **772**, 81–86.
24 D. T. Cramb and S. C. Beck, *J. Photochem. Photobiol., A*, 2000, **134**, 87–95.
25 A. W. Adamson, *Physical Chemistry of Surfaces*, Wiley, New York, 1990.